

# Mechanical cooling at the bistable regime of a dissipative optomechanical cavity with a Kerr medium

Ye Liu,<sup>1</sup> Yang Liu,<sup>1</sup> Chang-Sheng Hu,<sup>2</sup> Yun-Kun Jiang,<sup>1</sup> Huaizhi Wu,<sup>1</sup> and Yong Li<sup>3</sup>

<sup>1</sup>*Fujian Key Laboratory of Quantum Information and Quantum Optics and Department of Physics, Fuzhou University, Fuzhou 350116, China*

<sup>2</sup>*Department of Physics, Anhui Normal University, Wuhu 241000, China*

<sup>3</sup>*Center for Theoretical Physics, Hainan University, Haikou 570228, China*

In this paper, we study static bistability and mechanical cooling of a dissipative optomechanical cavity filled with a Kerr medium. The system exhibits optical bistability for a wide input-power range with the power threshold being greatly reduced, in contrast to the case of purely dissipative coupling. At the bistable regime, the membrane can be effectively cooled down to a few millikelvin from the room temperature under the unresolved sideband condition, where the effective mechanical temperature is a nonmonotonic function of intracavity intensity and reaches its minimum near the turning point of the upper stable branch. When the system is in the cryogenics environment, the effective mechanical temperature at the bistable regime shows a similar feature as in the room temperature case, but the optimal cooling appears at the monostable regime and approaches the mechanical ground state. Our results are of interest for further understanding bistable optomechanical systems, which have many applications in nonclassical state preparations and quantum information processing.

## I. INTRODUCTION

Cavity optomechanical systems, which study the interplay between light and mechanical motion, have important applications in fundamental tests of quantum mechanics, precision measurement, and quantum information processing [1]. For a generic setup, the radiation pressure force exerted by the light field typically induces a displacement-dependent cavity frequency, and thus enables a dispersive coupling between the optical and mechanical degrees of freedom. Since the radiation-pressure coupling is intrinsically nonlinear, optomechanical systems can exhibit different types of nonlinear behaviors, depending on the input power and the detuning of the driving laser with respect to the cavity resonance. In the blue-detuned regime, a strong driving can trigger rich nonlinear phenomena, such as dynamical multistability [2–7], instability [8], synchronization [6, 9–11], and chaotic motion [12–15]. In the red-detuned regime, one obtains the static optical bistability, where the mechanical mode in the low-temperature limit acts as a Kerr nonlinearity for the cavity mode [16]. The red-detuned regime is also considered as the appropriate regime for ground-state cooling of the mechanical motion [17–23], which is typically a prerequisite for nonclassical state preparation [24–29], quantum information processing [30–33], and quantum-limited measurements [34–39] with mechanical oscillators. With dispersive optomechanical coupling, sideband cooling of mechanical oscillation into its ground state has been experimentally demonstrated in the red-detuned regime out of the optical bistable region [20, 22, 40]. Besides, there are a few works which have also looked into the relationship between optical bistability and quantum effects. It has been shown that squeezing [41–47] and light-mechanical entanglement [48–50] induced

by optomechanical interactions become maximal for the parameter regime close to the threshold of the bistability or instability, and particularly, the entanglement is counter-intuitively not a monotonic function of the optomechanical coupling strength in the bistable region [48].

There exists another kind of cavity optomechanics [51–55], where the cavity linewidth depends on the mechanical displacement, giving rise to a dissipative coupling between the mechanical and the optical degrees of freedom. Dissipative optomechanical coupling can be realized with superconducting microwave circuits [51] or with a Michelson–Sagnac interferometer containing a semitransparent movable membrane [54, 56], and moreover, it has been experimentally demonstrated with a microdisc resonator coupled to a nanomechanical waveguide [57], with a photonic crystal split-beam nanocavity [58], and with graphene drums coupled to a high-Q microsphere [59]. In analogy to dispersive optomechanics, a dissipative coupling also allows for mechanical cooling [51, 60–62], nonclassical state preparation [63–68], quantum-limited position measurements [39, 69], and quantum sensing (of force [70–73] and speed [74, 75]). In contrast to purely dispersive systems, one can observe negative-damping instability [21, 51, 55, 56] and self-sustained oscillations [76] unconventionally for weak cavity driving of red detunings by involving a dissipative coupling. Although a purely dissipative coupling also has a nonlinear effect on the intracavity intensity, which is expected to show static bistability in principle [55], however, we note that the system is normally hard to run into bistability for typical experimental parameters with low input power [21]. Therefore, nonclassical properties of a dissipative optomechanical setup at the bistable regime may only be studied by introducing an extra nonlinearity or by considering a hybrid optomechanical system [77, 78].

In this paper, we study optical bistability and mechanical cooling at the bistable regime of a dissipative optomechanical system, which is implemented with a Michelson–Sagnac interferometer containing a movable membrane and a Kerr medium. We consider that the mechanical motion only causes a shift of the cavity damping rate, and does not vary the cavity frequency, corresponding to a purely dissipative coupling. As a clear advantage over the setting without Kerr nonlinearity, the cavity intensity can exhibit optical bistability at regular laser driving power of tens of milliWatt (mW), where the input-power-dependent cavity intensity displays a characteristic  $S$ -shaped curve and part of the upper branch of the curve turns unstable due to optomechanical coupling. In this regard, we note that the bistable region exists for a broad power range. In contrast, the optical bistability is sensitive to power fluctuation in typical dispersive systems [16, 48], and is inaccessible by the purely dissipative system with the Michelson–Sagnac interferometer and the input power of  $\sim 100$  mW. We then study mechanical cooling at the bistable regime, and find that the steady-state mechanical temperature is a non-monotonic function of intracavity intensity (or optomechanical coupling). The dissipative coupling allows the mechanical membrane to be effectively cooled from room temperature down to a few millikelvin in the unresolved sideband regime, and the optimal cooling condition appears at the upper branch close to the turning point. We further show that the membrane initially in a cryogenic environment of 0.1 K has similarly bistable features, and can be cooled down close to the ground state in the unresolved sideband regime for the case of only branch. Our findings are of interest for further studying the optomechanical nonclassical properties in the presence of static bistability.

The paper is organized as follows: Section II introduces the dissipative optomechanical system and describes the linearization of the equations of motion around the steady state. We also show the stability conditions required to satisfy in this framework. Section III introduces the effective mechanical susceptibility, noise spectrum and the effective temperature of the mechanical membrane. Section IV shows how bistability arises in the red-detuned regime, and the dependence of the photon number on the driving power and detuning, which leads us to a discussion of cooling on both stable branches in the bistable regime shown in Section V. Section VI is a further discussion and conclusion.

## II. MODEL, LINEARIZATION OF THE HAMILTONIAN, AND THE STABILITY CONDITION

As shown in Fig. 1, we consider an optomechanical Michelson-Sagnac interferometer [54], which includes a mechanical membrane (of mass  $m$ , frequency  $\omega_m$ , and damping rate  $\gamma_m$ ), and a Kerr medium (of

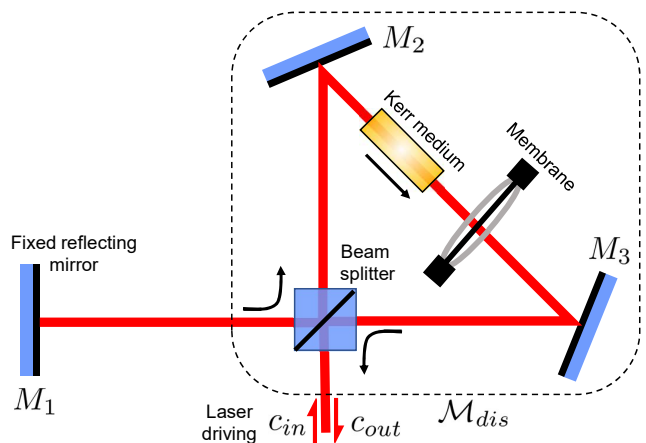


FIG. 1. (Color online) Schematics of the dissipative optomechanical setup. We consider a Michelson-Sagnac interferometer, which consists of three fixed perfect reflecting mirrors  $M_i$  ( $i = 1, 2, 3$ ) and a fixed beam splitter (BS). A movable membrane and a Kerr medium are placed in the middle of  $M_2$  and  $M_3$  [54]. A strong classical driving field is input to the interferometer via the vertical ports of the BS. The part encircled by dashed line can be regarded as an effective end mirror  $\mathcal{M}_{dis}$ . The linewidth of the cavity depends on the membrane displacement, which leads to an effective dissipative coupling between the cavity mode and the mechanical motion.

the nonlinearity strength  $U$ ) placed along the light propagation path. When an external driving field (with frequency  $\omega_l$  and power  $\mathcal{P}$ ) is injected into the interferometer at the beam splitter, the system can be effectively described as a dissipative optomechanical cavity, where the resonance frequency  $\omega_c(q)$  and decay rate  $\kappa(q)$  depend on the displacement of the mechanical membrane  $q$  [54]. The Hamiltonian of the system in a frame rotating at the input laser frequency  $\omega_l$  is given by [54]

$$H = \hbar[\omega_c(q) - \omega_l]c^\dagger c + \frac{1}{2}(m\omega_m^2 q^2 + \frac{p^2}{m}) + i\hbar\sqrt{2\kappa(q)} \times [c^\dagger(\epsilon_l + c_{in}) - c(\epsilon_l + c_{in}^\dagger)] - \hbar U c^{\dagger 2} c^2, \quad (1)$$

where  $c$  ( $c^\dagger$ ) is the annihilation (creation) operator of the cavity field satisfying the commutation relation  $[c, c^\dagger] = 1$ , and  $q$  and  $p$  are the mechanical displacement and momentum operators with  $[q, p] = i\hbar$ .  $\epsilon_l = \sqrt{\mathcal{P}/\hbar\omega_l}$  is the laser driving strength (assumed to be real for simplicity) and  $c_{in}$  is the input vacuum noise satisfying the usual nonvanishing correlation function  $\langle c_{in}(t)c_{in}^\dagger(t') \rangle = \delta(t - t')$ . Typically, the mechanical displacement only weakly modulates  $\omega_c(q)$  and  $\kappa(q)$  such that we can expand them to just the linear order of  $q$ , i.e. [51–55]

$$\omega_c(q) = \omega_c + g_\omega q, \quad \kappa(q) = \kappa + g_\kappa q,$$

where  $g_\omega = \partial\omega_c(q)/\partial q$  and  $g_\kappa = \partial\kappa(q)/\partial q$  are dispersive and dissipative coupling constants between the cavity

field and the membrane, respectively. Moreover, it has been shown that the dispersive coupling constant  $g_\omega$  can be set to zero if the complex reflectivity and transmissivity of the beam splitter are appropriately selected [54]. As a result, only the cavity decay rate depends on the mechanical displacement, and the setup is referred to as a (purely) dissipative optomechanical system. For the purely dissipative regime  $g_\omega = 0$ , the Hamiltonian of the system, in terms of the rescaled mechanical position and momentum operators  $Q = q/\sqrt{2x_{zpf}}$  and  $P = p(\sqrt{2x_{zpf}}/\hbar)$ , can be rewritten by

$$H = \hbar\Delta c^\dagger c + \frac{1}{2}\hbar\omega_m(Q^2 + P^2) - \hbar U c^{\dagger 2} c^2 + i\hbar\sqrt{2\kappa}\left(1 + \frac{g}{2\kappa}Q\right)[c^\dagger(\epsilon_l + c_{in}) - c(\epsilon_l + c_{in}^\dagger)], \quad (2)$$

where  $\Delta = \omega_c - \omega_l$  is the laser detuning with respect to the cavity resonant frequency, and  $g = \sqrt{2}g_\kappa x_{zpf}$  is the rescaled dissipative coupling constant.

From the above Hamiltonian, we can derive the detailed dynamics of the system via the standard Langevin equations

$$\begin{aligned} \dot{Q} &= \omega_m P, \\ \dot{P} &= -\omega_m Q - i\frac{g}{\sqrt{2\kappa}}[c^\dagger(\epsilon_l + c_{in}) - c(\epsilon_l + c_{in}^\dagger)] \\ &\quad - \gamma_m P + \xi, \\ \dot{c} &= -(\kappa + gQ + i\Delta)c + \sqrt{2\kappa}\left(1 + \frac{g}{2\kappa}Q\right)(\epsilon_l + c_{in}) \\ &\quad + 2iUc^{\dagger 2}c^2, \end{aligned} \quad (3)$$

where the mechanical thermal noise  $\xi$  is zero mean valued and fulfills the two-time correlation function  $\langle \xi(t)\xi(t') \rangle = \frac{1}{2\pi} \frac{\gamma_m}{\omega_m} \int \omega e^{-i\omega(t-t')} [1 + \coth(\frac{\hbar\omega}{2k_B T})] d\omega$  [79, 80], with  $T$  being the thermal temperature of the environment. By denoting  $\bar{O} = \langle O \rangle$  as the steady-state value of  $O = Q, P, c$ , and using the fact  $\langle c_{in} \rangle = 0$  and  $\langle \xi \rangle = 0$ , one can obtain the steady-state semiclassical solutions of  $\bar{O}$  by solving Eq. (3) with  $\langle \dot{O} \rangle = 0$ , which gives rise to

$$\bar{Q} = ig\sqrt{\mathcal{P}_l} \frac{(\bar{c} - \bar{c}^*)}{\omega_m}, \quad \bar{P} = 0, \quad (4)$$

$$\bar{c} = \frac{(\kappa + \tilde{\kappa})\sqrt{\mathcal{P}_l}}{\tilde{\kappa} + i(\Delta - 2U|\bar{c}|^2)}, \quad (5)$$

with  $\tilde{\kappa} = \kappa + g\bar{Q}$ , and  $\mathcal{P}_l = \epsilon_l^2/2\kappa$ . Eq. (5) implies that a static bistability may occur even though the Kerr nonlinearity is set to zero [55]. However, we find that the system cannot run into bistability for the typical experimental parameters with the input power of a few hundred mW [21]. Thus, the Kerr nonlinearity is of great essential for the bistable regime focused on in this work.

Assuming that the mean photon number in the cavity is far more than 1 (i.e.  $\langle c^\dagger c \rangle \gg 1$ ), and the static stability conditions (shown later) are met, we proceed with the usual linearization around steady state by decomposing

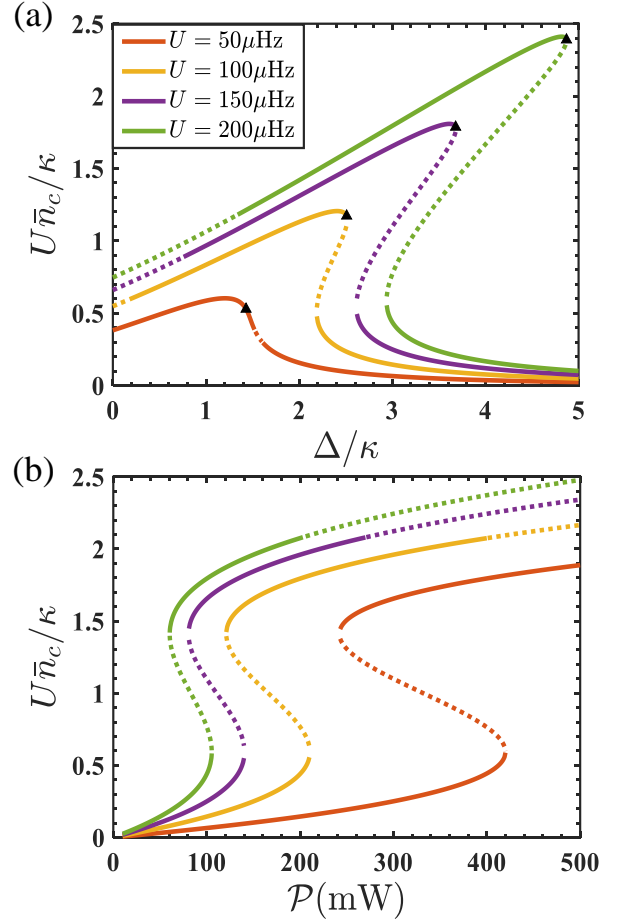


FIG. 2. (Color online) The normalized cavity intensity  $U\bar{n}_c/\kappa$  (a) as a function of the dimensionless detuning  $\Delta/\kappa$  for driving power  $\mathcal{P} = 100$  mW, and (b) as a function of the driving power  $\mathcal{P}$  for  $\Delta/\kappa = 3$ , with the nonlinearity strengths being  $U = 50$   $\mu\text{Hz}$  (orange), 100  $\mu\text{Hz}$  (yellow), 150  $\mu\text{Hz}$  (purple) and 200  $\mu\text{Hz}$  (green), respectively. We consider the set of typical experimental parameters [21]: the wavelength of the input laser  $\lambda = 2\pi c/\omega_l = 1064$  nm, the cavity decay rate  $\kappa = 2\pi \times 1.5$  MHz, the dissipative optomechanical coupling rate  $g = 2\pi \times 0.1$  Hz, the mechanical frequency  $\omega_m = 2\pi \times 136$  kHz, and the mechanical damping rate  $\gamma_m = 2\pi \times 0.23$  Hz. The cavity intensity displays a characteristic S-shaped curve, with the stable and unstable parts being indicated by the solid and dotted lines, respectively. The black triangles mark the parameter conditions plotted in Fig. 3.

each observable as the sum of its steady-state mean value and a small quantum fluctuation:  $O = \bar{O} + \delta O$ . Neglecting higher order terms for the fluctuations, we

obtain

$$\begin{aligned}
\delta\dot{Q} &= \omega_m \delta P, \\
\delta\dot{P} &= -\omega_m \delta Q + i \frac{g\epsilon_l}{\sqrt{2\kappa}} (\delta c - \delta c^\dagger) - \gamma_m \delta P \\
&\quad - i \frac{g}{\sqrt{2\kappa}} (\bar{c}^* c_{in} - \bar{c} c_{in}^\dagger) + \xi, \\
\delta\dot{c} &= -(\tilde{\kappa} + i\tilde{\Delta})\delta c + g\zeta\delta Q + 2i\tilde{U}e^{i\phi}\delta c^\dagger \\
&\quad + \frac{1}{\sqrt{2\kappa}}(\kappa + \tilde{\kappa})c_{in}, \tag{6}
\end{aligned}$$

where  $\tilde{U} = U|\bar{c}|^2$ ,  $\tilde{\Delta} = \Delta - 4\tilde{U}$ ,  $\phi = \arg(\bar{c}^2)$  and  $\zeta = \sqrt{\mathcal{P}_l} - \bar{c}$ . The Kerr nonlinearity introduces two effects to

the system: First, the cavity field  $\delta c$  can be squeezed via the parametric Hamiltonian  $-\hbar\tilde{U}e^{i\phi}\delta c^{\dagger 2} + \text{H.c.}$ ; second, the cavity frequency is effectively shifted by  $4\tilde{U}$ , which is essential for stabilization of the system to achieve mechanical cooling. To examine the dynamic stability of the system, we further rewrite the Langevin equations by  $\dot{u}(t) = Mu(t) + n(t)$ , which are expressed in terms of the quadrature operators  $u(t) = [\delta Q, \delta P, \delta x, \delta y]^T$  with  $\delta x = \frac{1}{\sqrt{2}}(\delta c + \delta c^\dagger)$  and  $\delta y = \frac{1}{\sqrt{2}i}(\delta c - \delta c^\dagger)$  being the amplitude and phase quadratures of the cavity field,  $n(t) = [0, \xi + \frac{g}{\sqrt{2\kappa}}(-\bar{c}_i x_{in} + \bar{c}_r y_{in}), \frac{\kappa + \tilde{\kappa}}{\sqrt{2\kappa}} x_{in}, \frac{\kappa + \tilde{\kappa}}{\sqrt{2\kappa}} y_{in}]^T$  with  $x_{in} = \frac{1}{\sqrt{2}}(c_{in} + c_{in}^\dagger)$  and  $y_{in} = \frac{1}{\sqrt{2}i}(c_{in} - c_{in}^\dagger)$  being the input vacuum noises, and the evolution matrix

$$M = \begin{pmatrix} 0 & \omega_m & 0 & 0 \\ -\omega_m & -\gamma_m & 0 & -g\sqrt{2\mathcal{P}_l} \\ \sqrt{2}g(\sqrt{\mathcal{P}_l} - \bar{c}_r) & 0 & -\tilde{\kappa} - 2\tilde{U}\sin\phi & \tilde{\Delta} + 2\tilde{U}\cos\phi \\ -\sqrt{2}g\bar{c}_i & 0 & -\tilde{\Delta} + 2\tilde{U}\cos\phi & -\tilde{\kappa} + 2\tilde{U}\sin\phi \end{pmatrix} \tag{7}$$

with  $\bar{c}_r = \frac{1}{2}(\bar{c} + \bar{c}^*)$ ,  $\bar{c}_i = \frac{1}{2i}(\bar{c} - \bar{c}^*)$ . Followed by a consideration of the Routh-Hurwitz criterion [81], the

real part of the eigenvalues of  $M$  should be strictly negative such that the system is stable, which gives rise to the stability conditions below:

$$s_1 = 2\tilde{\kappa}[(\tilde{\kappa} + \gamma_m)^2 + \tilde{\Delta}^2 - 4\tilde{U}^2] + 2\sqrt{\mathcal{P}_l}g^2\bar{c}_i\omega_m + \gamma_m\omega_m^2 > 0, \tag{8}$$

$$s_2 = 2\sqrt{\mathcal{P}_l}g^2[(\bar{c}_r - \sqrt{\mathcal{P}_l})(\tilde{\Delta} - 2\tilde{U}\cos\phi) - \bar{c}_i(\tilde{\kappa} + 2\tilde{U}\sin\phi)] + (\tilde{\kappa}^2 + \tilde{\Delta}^2 - 4\tilde{U}^2)\omega_m > 0, \tag{9}$$

$$s_3 = s_1[(\tilde{\kappa}^2 + \tilde{\Delta}^2 - 4\tilde{U}^2)\gamma_m + 2\omega_m(\tilde{\kappa}\omega_m - \sqrt{\mathcal{P}_l}g^2\bar{c}_i)] - (2\tilde{\kappa} + \gamma_m)^2 s_2 \omega_m > 0. \tag{10}$$

Moreover, since the studies of the current work focus on the bistable regime, we have to also confirm that the fluctuation of photon number is much less than the classical mean value, i.e.  $(\langle c^\dagger c \rangle - |\bar{c}|^2)/|\bar{c}|^2 \ll 1$ , such that our discussions stay within the range of validity of the linearization approximation.

### III. OPTICAL BISTABILITY

According to Eq. (5), we obtain a third-order polynomial root equation for the mean-field cavity occupation.

$$4U^2\bar{n}_c^3 - 4\Delta U\bar{n}_c^2 + (\tilde{\kappa}^2 + \Delta^2)\bar{n}_c = \mathcal{P}_l(\kappa + \tilde{\kappa})^2, \tag{11}$$

where  $\bar{n}_c = |\bar{c}|^2$ . Equation (11) indicates that the steady-state cavity intensity  $\bar{n}_c$  can have either one or three solutions, depending on the number of real roots of the polynomial. By considering the parameter regime,

where the mechanical frequency and damping rate are  $(\omega_m, \gamma_m)/\kappa = (0.091, 1.53 \times 10^{-7})$ , the optomechanical coupling strength is  $g/\kappa = 6.67 \times 10^{-8}$ , the cavity driving strength is  $\epsilon_l^2/\kappa = 5.68 \times 10^{10}$ , in Fig. 2(a), we plot the rescaled mean-field occupation  $U\bar{n}_c/\kappa$  as a function of the detuning  $\Delta/\kappa$  for  $\kappa = 2\pi \times 1.5$  MHz and then the driving power  $\mathcal{P} = \epsilon_l^2(\hbar\omega_l) = 100$  mW. As the Kerr nonlinearity increases from  $U = 50$   $\mu\text{Hz}$  ( $U/\kappa = 0.53 \times 10^{-11}$ ) to  $U = 200$   $\mu\text{Hz}$  ( $U/\kappa = 2.12 \times 10^{-11}$ ), the cavity line shape, which is approximately Lorentzian for  $U = 0$ , becomes more and more asymmetric and tilts until. The system is stable only when the stability criteria Eqs. (8)-(10) are obeyed. In general, the violation of the criterion  $s_1 > 0$  and  $s_2 > 0$  always yields an unstable middle branch, while the additional criterion for the optomechanical system  $s_3 > 0$  can turn part of the upper or only branch unstable, see the tails near the resonance  $\Delta/\kappa = 0$ .

Since part of the upper branch of the  $S$ -shaped curves may turn unstable and the system can be in the

monostable regime for  $\Delta/\kappa \rightarrow 0$  with the parameters under consideration, in Fig. 2(b), we plot the rescaled mean-field occupation  $U\bar{n}_c/\kappa$  as a function of the driving power  $\mathcal{P}$  for the fixed detuning  $\Delta/\kappa = 3$ . For an increasing driving power  $\mathcal{P}$ , in all cases the mean-field occupations  $\bar{n}_c$  have three branches, which form a characteristic  $S$ -shaped curve. As discussed before, the violation of  $\{s_1, s_2\} > 0$  again gives rise to an unstable middle branch, and the upper branch is stable only in a finite segment corresponding to  $s_3 > 0$ . Note that for a large detuning  $\Delta/\kappa \gg 3$  (and for the nonlinearity strengths under consideration), it requires a far stronger driving to exhibit optical bistability, and meanwhile the laser detuning itself must remain far less than the free spectral range of the cavity.

Without optomechanical coupling, the Kerr nonlinearity can lead to optical bistability with a fully stable upper branch [16]; with purely dissipative optomechanical coupling but without the Kerr nonlinearity, the bistable behavior can only turn up at the strong laser driving power of a few Watts, which is normally hard to access for typical quantum optical experiments. Here, by combining the Kerr nonlinearity with the dissipative coupling interaction, we are able to observe optical bistability at the driving power on the order of  $\sim 100$  mW, and moreover, the optical bistability is much less insensitive to power fluctuation, in contrast to that in dispersive optomechanical systems with typical parameters (as shown by Aldana et al. [16]), which is confined in a power range of a few mW due to the limit of the stability condition  $s_3$ , and therefore is sensitive to power disturbance.

Recalling that the resonant frequency of the cavity can be shifted by  $\sim U\bar{n}_c$  because of the Kerr nonlinearity, here we have carefully examined the effective detunings  $\tilde{\Delta} = \Delta - 4U\bar{n}_c$ , which is in the range of  $-5 < \tilde{\Delta}/\kappa < 5$  with respect to the  $S$ -shaped curves in Fig. 2(b), and confirmed that both  $\Delta$  and  $\tilde{\Delta}$  remain far less than the free spectral range of the cavity, which is given by  $\text{FSR} = c/(2L) = 1.7 \text{ GHz} \sim 180\kappa$  with the effective cavity length  $L = 0.087 \text{ m}$  and the cavity decay rate  $\kappa/2\pi \sim 1.5 \text{ MHz}$  [21].

#### IV. EFFECTIVE MECHANICAL SUSCEPTIBILITY, NOISE SPECTRUM, AND FINAL TEMPERATURE

In order to gain more insights into the dynamics of the system and the limitations for effective cooling of the membrane, we analytically derive the effective mechanical susceptibility and the spectra of the input noises. We first Fourier transform Eq. (6) by using  $\delta O(\omega) = \int_{-\infty}^{+\infty} \delta O(t) e^{i\omega t} d\omega$ , after simple algebra, then obtain the expression of the position fluctuations in the

frequency domain,

$$\delta Q(\omega) = \chi_{\text{eff}}(\omega) \left[ \Lambda(\omega) c_{\text{in}}(\omega) + \Lambda^*(-\omega) c_{\text{in}}^\dagger(\omega) + \xi(\omega) \right], \quad (12)$$

where

$$\chi_{\text{eff}}^{-1}(\omega) = \chi_m^{-1}(\omega) + \Xi(\omega) \quad (13)$$

is the effective mechanical susceptibility with

$$\chi_m^{-1}(\omega) = \frac{\omega_m^2 - i\omega\gamma_m - \omega^2}{\omega_m}, \quad (14)$$

$$\Xi(\omega) = -i\sqrt{\mathcal{P}_l} g^2 \frac{\tilde{\chi}_c^{-1}(\omega)\zeta - [\tilde{\chi}_c^{-1}(-\omega)]^* \zeta^*}{\chi_c^{-1}(\omega) [\chi_c^{-1}(-\omega)]^* - 4\tilde{U}^2}, \quad (15)$$

$$\chi_c^{-1}(\omega) = \tilde{\kappa} - i(\omega + \tilde{\Delta}), \quad (16)$$

$$\tilde{\chi}_c^{-1}(\omega) = \chi_c^{-1}(\omega) + 2i\tilde{U}e^{-i\phi}, \quad (17)$$

and

$$\Lambda(\omega) = i\frac{g}{\sqrt{2\kappa}} \left[ \frac{\sqrt{\mathcal{P}_l}(\kappa + \tilde{\kappa})\tilde{\chi}_c^{-1}(\omega)}{\chi_c^{-1}(\omega) [\chi_c^{-1}(-\omega)]^* - 4\tilde{U}^2} - \bar{c}^* \right]. \quad (18)$$

Eq. (12) shows that the mechanical fluctuations are given by the product of the effective susceptibility  $\chi_{\text{eff}}(\omega)$  and the sum of fluctuations arising from two uncorrelated noise terms, namely the back action force noise of the cavity mode and the mechanical Brownian noise. Moreover, the effects of the dissipative optomechanical coupling  $g$  and the Kerr nonlinearity  $U$  have been collected into the quantity  $\Xi(\omega)$ , which may be called as the optomechanical self-energy [2]. Since the dissipative coupling is weak ( $g/\kappa \ll 1$ ), the effective susceptibility  $\chi_{\text{eff}}(\omega)$  will have a single resonance, whose property is just modified by the presence of the Kerr nonlinearity  $U$ . To see the physical insight, we then rewrite the effective mechanical susceptibility as

$$\chi_{\text{eff}}(\omega) = \frac{\omega_m}{\omega_{\text{eff}}^2 - \omega^2 - i\omega\gamma_{\text{eff}}(\omega)}, \quad (19)$$

where

$$\omega_{\text{eff}}^2(\omega) - \omega_m^2 = -\frac{g^2\sqrt{\mathcal{P}_l}\omega_m\mu}{\lambda^2(\omega) + 4\omega^2\tilde{\kappa}^2} \quad (20)$$

and

$$\gamma_{\text{eff}}(\omega) - \gamma_m = \frac{g^2\sqrt{\mathcal{P}_l}\omega_m\nu}{\lambda^2(\omega) + 4\omega^2\tilde{\kappa}^2}, \quad (21)$$

with

$$\lambda(\omega) = \tilde{\kappa}^2 + \tilde{\Delta}^2 - \omega^2 - 4\tilde{U}^2,$$

$$\mu = -2\text{Im} [\tilde{\chi}_c^{-1}(0)\zeta] \lambda(\omega) + 4\omega^2\tilde{\kappa}\tilde{c}_i,$$

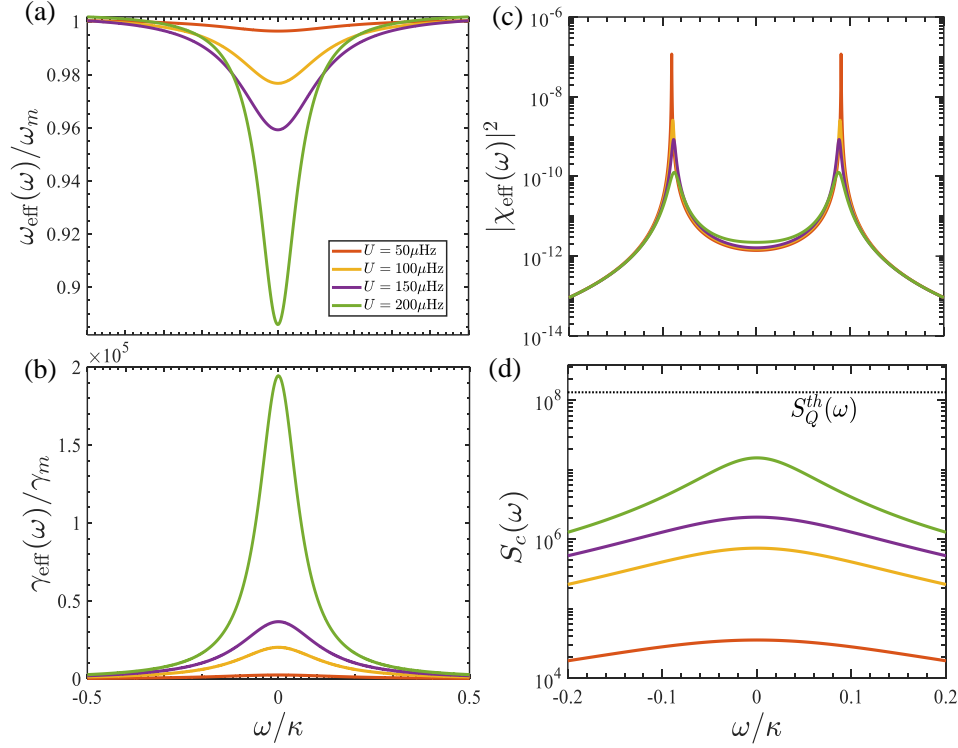


FIG. 3. (Color online) (a) The normalized effective resonance frequency  $\omega_{\text{eff}}(\omega)/\omega_m$ , (b) the normalized effective damping rate  $\gamma_{\text{eff}}(\omega)/\gamma_m$ , (c) the modulus of effective susceptibility  $|\chi_{\text{eff}}(\omega)|^2$ , and (d) spectrum of the input vacuum noise as a function of the normalized frequency  $\omega/\kappa$ . The dotted line in (d) indicates the mechanical thermal noise, which for the environment of the room temperature  $T = 293$  K considered here is approximately frequency independent. The Kerr nonlinearity and the cavity detuning for the curves [from top to bottom in (a)] are  $U = 50 \mu\text{Hz}$  and  $\Delta = 1.43\kappa$  (orange),  $U = 100 \mu\text{Hz}$  and  $\Delta = 2.51\kappa$  (yellow),  $U = 150 \mu\text{Hz}$  and  $\Delta = 3.68\kappa$  (purple),  $U = 200 \mu\text{Hz}$  and  $\Delta = 4.87\kappa$  (green), respectively, corresponding to the parameters indicated by the black triangles in Fig. 2(a). Other parameters are the same as in Fig. 2.

$$\nu = -2\lambda(\omega)\bar{c}_i - 4\tilde{\kappa}\text{Im}[\tilde{\chi}_c^{-1}(0)\zeta].$$

By comparing Eq. (13) with Eq. (19), one can figure out the meaning of both the imaginary and the real parts of  $\Xi(\omega)$ , which evaluated at the original resonance frequency  $\omega = \omega_m$  are a shift of the mechanical frequency (“optical spring”) and some optomechanical damping rate, respectively [17, 18].

Furthermore, by considering the nonzero correlation functions  $\langle c_{\text{in}}(\omega)c_{\text{in}}^\dagger(\omega') \rangle = 2\pi\delta(\omega - \omega')$  and  $\langle \xi(\omega)\xi(\omega') \rangle = 2\pi\frac{\gamma_m}{\omega_m}\omega[1 + \coth(\frac{\hbar\omega}{2k_B T})]\delta(\omega - \omega')$  for the noise operators, we obtain the spectrum of the mechanical position and momentum [68],

$$S_Q(\omega) = |\chi_{\text{eff}}(\omega)|^2 [S_c(\omega) + S_Q^{\text{th}}(\omega)], \quad (22)$$

$$S_P(\omega) = \frac{\omega^2}{\omega_m^2} S_Q(\omega), \quad (23)$$

where  $S_c(\omega) = \frac{1}{2}[\Lambda(\omega)\Lambda^*(\omega) + \Lambda(-\omega)\Lambda^*(-\omega)]$  and  $S_Q^{\text{th}}(\omega) = \frac{\gamma_m}{\omega_m}\omega\coth(\frac{\hbar\omega}{2k_B T})$  are spectra of the input vacuum noise and the mechanical thermal noise, respectively. Integrating  $S_Q(\omega)$  and  $S_P(\omega)$  over all the

frequency range then gives rise to the variance of the mechanical position and momentum:

$$\langle \delta Q^2 \rangle = \frac{1}{2\pi} \int_{-\infty}^{+\infty} d\omega S_Q(\omega), \quad (24)$$

$$\langle \delta P^2 \rangle = \frac{1}{2\pi} \int_{-\infty}^{+\infty} d\omega S_P(\omega). \quad (25)$$

As a figure of merit for cooling, we calculate the final occupation number of the mechanical membrane via

$$n_m = \frac{1}{2}[\langle \delta Q^2 \rangle + \langle \delta P^2 \rangle - 1], \quad (26)$$

and consider the effective temperature in the membrane with

$$T_{\text{eff}} = \frac{\hbar\omega_m}{k_B \ln(1 + \frac{1}{n_m})}. \quad (27)$$

In addition, by following the same recipe as from Eq. (22) to Eq. (26), we can further calculate the variance of the amplitude and phase quadratures of the cavity field, which enables us to examine optical squeezing and the fluctuation of the photon number above its classical

mean value  $\bar{n}_c$  via  $\delta n_c = \frac{1}{2}[\langle \delta x^2 \rangle + \langle \delta y^2 \rangle - 1]$ . The latter is then used to confirm the validity of the linearization approximation, which is a prerequisite for the discussion of mechanical cooling at the bistable regime.

## V. MECHANICAL COOLING IN THE BISTABLE REGION

We now focus on the mechanical cooling in the bistable regime or in the vicinity of the unstable part for the case of only branch. In the bistable regime, the fluctuation  $\delta n_c$  in cavity intensity around the steady state solution  $\bar{n}_c$  may diverge as one approaches the end of each stable branch. In order to stay within the range of validity of the linearization approximation, we have confirmed  $\delta n_c / \bar{n}_c \ll 1$  for the results shown below, see further discussions later. In Figs. 3(a) and 3(b), we show the normalized effective resonance frequency  $\omega_{\text{eff}}(\omega)/\omega_m$  and the normalized effective damping rate  $\gamma_{\text{eff}}(\omega)/\gamma_m$  of the membrane as functions of the normalized frequency  $\omega/\kappa$  for different strengths of the Kerr nonlinearity  $U = \{50, 100, 150, 200\}$   $\mu\text{Hz}$ , where the corresponding cavity detunings are  $\Delta/\kappa = 1.43, 2.51, 3.68,$  and  $4.87$ , respectively. It can be seen that the overall profiles of  $\omega_{\text{eff}}(\omega)/\omega_m$  for all values of  $U$  are above 0.88. As the Kerr nonlinearity increases, the optomechanically induced frequency shift  $\omega_{\text{eff}}(0)/\omega_m$ , and correspondingly, the modified damping rate  $\gamma_{\text{eff}}(0)/\gamma_m$  gets larger. Moreover, the responses of  $\omega_{\text{eff}}(\omega)/\omega_m$  to optomechanical interaction around the mechanical resonance (i.e.,  $\omega = \omega_m \sim 0.091\kappa$ ) can be larger than 0.96, with the modified damping rate  $\gamma_{\text{eff}}(\omega)$  increasing to  $\sim 2\pi \times 0.02$  MHz for  $U = 200$   $\mu\text{Hz}$ . It implies that the optomechanically induced cooling of the membrane can be realized with a relatively small ‘‘optical spring’’ frequency shift for the set of Kerr nonlinearity  $U = \{50, 100, 150, 200\}$   $\mu\text{Hz}$  under consideration.

*Room temperature* - We first suppose that the membrane is in the room temperature environment with  $T = 293$  K, which corresponds to the thermal phonon number of the membrane  $n_m = 4.49 \times 10^7$  according to  $n_m = (e^{\hbar\omega_m/k_B T} - 1)^{-1}$ . In this case, the achievable final phonon number by optomechanical cooling is limited by the input vacuum noise  $c_{\text{in}}(\omega)$  and the mechanical thermal noise  $\xi(\omega)$ , which make effects via the response function (i.e., the modulus of the effective susceptibility)  $|\chi_{\text{eff}}(\omega)|^2$ , see Eqs. (12) and (22). As shown in Fig. 3(c),  $|\chi_{\text{eff}}(\omega)|^2$  displays two peaks at  $\omega = \pm\omega_{\text{eff}}(\omega_m)$ , and the full width at half maximum (FWHM) of the peaks is determined by  $\gamma_{\text{eff}}(\omega)$ . The response function  $|\chi_{\text{eff}}(\omega)|^2$  ensures that the noise spectrum is only significant around a narrow bandwidth centered about  $\pm\omega_{\text{eff}}(\omega_m)$ . Furthermore, the spectrum  $S_c(\omega)$  of the input vacuum noise is maximized at the cavity resonance  $\omega = 0$ , and the spectrum  $S_Q^{th}(\omega)$  of the thermal noise at the thermal temperature  $T = 293$  K is almost flat in the frequency range  $\omega/\kappa \in (-0.2, 0.2)$ , see Fig. 3(d). By comparison,

the thermal noise at room temperature dominates over the vacuum noise from the cavity input. As a result, the position spectrum  $S_Q(\omega)$  of the membrane can be approximately given by

$$S_Q(\omega) \approx |\chi_{\text{eff}}(\omega)|^2 \left( \frac{2k_B T}{\hbar\omega_m} + 1 \right) \gamma_m, \quad (28)$$

which is the response function  $|\chi_{\text{eff}}(\omega)|^2$  multiplied by a constant factor of the damping rate  $(2k_B T/\hbar\omega_m + 1)\gamma_m$  induced by the bath with temperature  $T$ . Thus, the position spectrum  $S_Q(\omega)$  displays two peaks at  $\omega = \pm\omega_{\text{eff}}(\omega_m)$  as well, and holds the linewidths  $\gamma_{\text{eff}}(\omega_m)$  similar to  $|\chi_{\text{eff}}(\omega)|^2$ . When the strength of the Kerr nonlinearity increases [with the parameters being the same as in Fig. 3(a)], the peak values of  $|\chi_{\text{eff}}(\omega)|^2$  and therefore  $S_Q(\omega)$  decrease sharply, while the corresponding FWHMs broaden, see Fig. 3(c).

Considering the room temperature condition and the unresolved sideband limit, the final phonon number is then given by

$$n_m \approx \frac{k_B T \gamma_m}{2\pi \hbar \omega_m} \int_{-\infty}^{+\infty} d\omega \left( 1 + \frac{\omega^2}{\omega_m^2} \right) |\chi_{\text{eff}}(\omega)|^2 - \frac{1}{2}. \quad (29)$$

Before we present the cooling effect, in Fig. 4(a), we first show the phase diagram of the stable regimes (defined by the Routh-Hurwitz criterion) as a function of the dimensionless detuning  $\Delta/\kappa$  and the effective optical gain  $\tilde{U}/\kappa$ . Previously, we have shown that the violation of the conditions  $s_j > 0$  ( $j = 1, 2, 3$ ) has related to the stability of the upper or middle branch when optical bistability occurs. Now, the cooling results are particularly interesting because the effective mechanical temperature  $T_{\text{eff}}$  also strongly relies on the specific condition being violated, as shown in Fig. 4(b). For further insights, we have also shown  $\tilde{U}$  as a function of  $\Delta/\kappa$  with the Kerr nonlinearity strengths being  $U = \{50, 100, 150, 200\}$   $\mu\text{Hz}$ , namely the S-shaped curves shown in Fig. 2(a). For the cases of optical bistability, it is worth noting that  $T_{\text{eff}}$  gradually goes down as  $s_1$  or  $s_2$  approaches zero and suddenly surges near  $s_{1(2)} \approx 0$  accompanied by divergence of  $\delta n_c$  (see discussion later);  $T_{\text{eff}}$  reaches less than 5 mK in the vicinity of the turning point at the upper branch. Indeed, this can be understood with the optomechanical damping rate  $(\gamma_{\text{eff}}(\omega) - \gamma_m)$  [as given by Eq. (21)], which can lead to extra damping and mechanical cooling when  $(\gamma_{\text{eff}}(\omega) - \gamma_m)$  is positive [17, 18]. Recalling that  $S_Q(\omega)$  is approximately given by the product of  $|\chi_{\text{eff}}(\omega)|^2$  and the constant damping rate  $\left( \frac{2k_B T}{\hbar\omega_m} + 1 \right) \gamma_m$ , then for the frequency shift  $(\omega_{\text{eff}} - \omega_m)$  being small and  $\gamma_{\text{eff}} \ll \kappa$ , one can approach the best cooling effect by minimizing  $|\chi_{\text{eff}}(\omega)|^2 \approx \gamma_{\text{eff}}^{-2}(\omega)$  [or maximizing  $(\gamma_{\text{eff}}(\omega) - \gamma_m)$ ] with  $\omega = \omega_m$ . Thus, we set  $\lambda(\omega_m) = 0$  to minimize the denominator of Eq. (21), and find that  $\tilde{\kappa}^2 + \tilde{\Delta}^2 - \omega_m^2 - 4\tilde{U}^2 = 0$  fits approximately with the boundary of the unstable region corresponding to  $s_{1(2)} < 0$  [as indicated by the black dash-dotted line

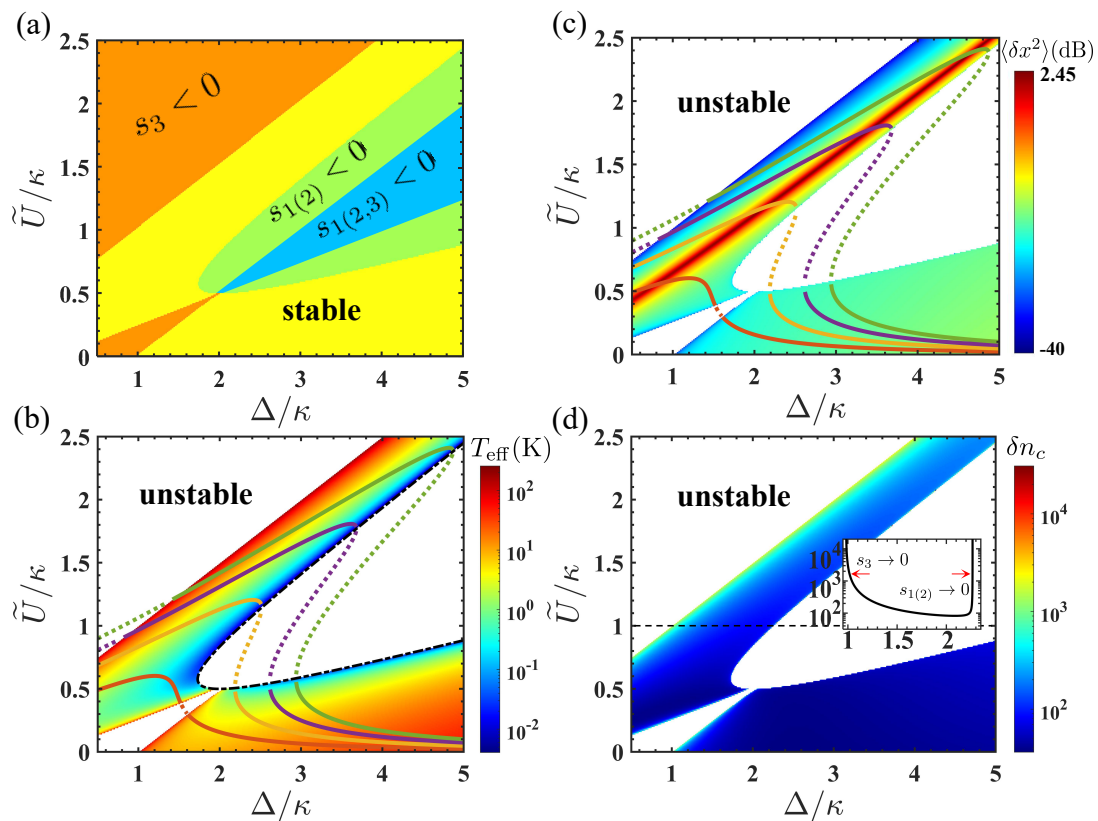


FIG. 4. (Color online) (a) Phase diagram of the stable regime (yellow) confirmed via the Routh-Hurwitz criterion, which requires  $s_1$ ,  $s_2$  and  $s_3$  to be all positive. The unstable region in green corresponds to  $s_1 < 0$  (or  $s_2 < 0$ ), and the orange region corresponds to  $s_3 < 0$ . In the blue region,  $s_1$ ,  $s_2$ , and  $s_3$  are all negative. (b) Effective temperature of the membrane in the steady state versus  $\Delta/\kappa$  and  $\tilde{U}/\kappa$  by cooling from the initial room temperature  $T = 293$  K. The black dash-dotted line indicates  $\lambda(\omega_m) = 0$ , which fits approximately with the boundary of the unstable region with  $s_{1(2)} < 0$ , corresponding to the green zone in (a). (c) Variance of the optical quadrature fluctuation  $\langle \delta x^2 \rangle$  and (d) the photon number fluctuation  $\delta n_c$  versus  $\Delta/\kappa$  and  $\tilde{U}/\kappa$ . The inset shows  $\delta n_c$  versus  $\Delta/\kappa$  for  $\tilde{U}/\kappa = 1$ , and the photon number fluctuation diverges at the stability boundary with  $s_j \rightarrow 0$ ,  $j = 1, 2, 3$ . In (b)-(d), the blank regions correspond to the classical unstable regime. The four curves [in (b), (c)], and other parameters are the same as those in Fig. 2(a).

in Fig. 4(b)], and moreover  $\gamma_{\text{eff}}(\omega_m)$  is large near the boundary. In contrast, for the tails of the curves close to  $\Delta = 0$  and for the case of only branch, as  $s_3$  approaches zero (i.e. the violation of the stability condition  $s_3$ ), we find that  $\lambda^2(\omega_m) \gg 4\omega_m^2 \tilde{\kappa}^2$  and  $v(\omega_m) \rightarrow 0$ , and thus  $T_{\text{eff}}$  quickly goes up due to a vanishing optomechanical damping rate ( $\gamma_{\text{eff}}(\omega_m) - \gamma_m$ ). Here, the linearization approximation is not justified and mechanical lasing instability may occur [2, 4, 5]. The lowest temperature of the membrane reached by combining the dissipative coupling and the Kerr interaction is about three orders of magnitude lower than that without the Kerr medium (i.e.  $U = 0$ ).

The Kerr nonlinearity can bring about not only the optical bistability, but also a parametric amplification. To see that, we show the variance of the  $x$  quadrature of the cavity field in Fig. 4(c). We find that the intracavity squeezing of about 2.43 dB can be generated around  $\Delta \approx 2\tilde{U}$  in both the monostable and the bistable regime. For the cases of  $U = 50$   $\mu\text{Hz}$  and

$U = 100$   $\mu\text{Hz}$ , the intracavity squeezing appears in the monostable region around  $\Delta/\kappa = 0.78$  and  $\Delta/\kappa = 2.15$ , and the steady-state mechanical temperatures are 1.38 K and 0.77 K, respectively. For  $U = 150$   $\mu\text{Hz}$  and  $U = 200$   $\mu\text{Hz}$ , the intracavity squeezing appears in the bistable region and is only related to the upper branch, the steady-state mechanical temperatures are 0.52 K and 0.4 K with  $\Delta/\kappa = 3.43$  and  $\Delta/\kappa = 4.68$ , respectively. Although the mechanical temperature can also reach the same level  $\sim 0.1$  K at the lower branch, the variance in the  $x$ -quadrature (or the  $y$ -quadrature) does not approach the zero-point level anymore. On the other hand, as mentioned before,  $\delta n_c \ll \bar{n}_c$  should hold for the effectiveness of the linearized dynamics, however, as  $s_j$  ( $j = 1, 2, 3$ ) approaches zero the variance in the  $x$ -quadrature (or  $y$ -quadrature) and the photon number fluctuation  $\delta n_c$  diverge, then the linearization approximation is not justified anymore. As indicated in Fig. 4(d),  $\delta n_c$  is a few tens or a few hundreds of quanta in most of the stable regions, and becomes larger

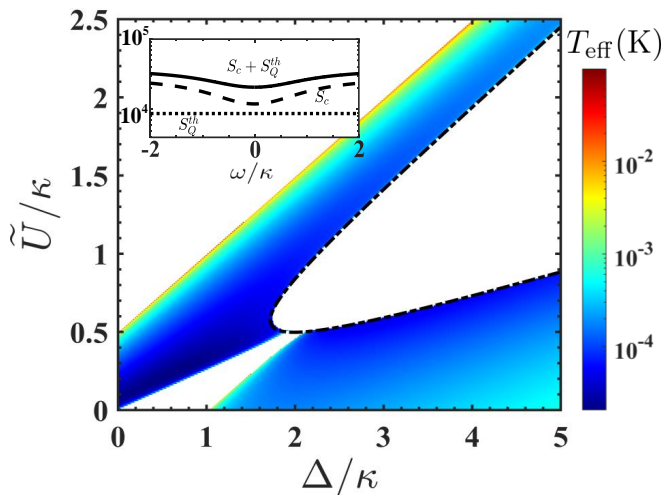


FIG. 5. (Color online) Effective temperature of the membrane in the steady state versus  $\Delta/\kappa$  and  $\tilde{U}/\kappa$  by cooling from the initial cryogenic temperature  $T = 0.1$  K. The blank regions correspond to the classical unstable regime confirmed via the Routh-Hurwitz criterion. The black dash-dotted line indicates  $\lambda(\omega_m) = 0$ . The inset shows the spectra of the input vacuum noise  $S_c(\omega)$  (dashed), the thermal noise  $S_Q^{th}(\omega)$  (dotted), and sum of them (solid). Other parameters are  $(\kappa, g, \omega_m, \gamma_m)/2\pi = (1.5 \text{ MHz}, 0.35 \text{ Hz}, 300 \text{ kHz}, 0.1 \text{ Hz})$  and  $\mathcal{P} = 100 \text{ mW}$ .

than  $10^3$  only at the boundary with  $s_j \rightarrow 0$ . Moreover, the inset shows that  $\delta n_c$  increases more sharply at the turning point with  $(s_{1(2)} \rightarrow 0)$ , near the optimal cooling regime.

*Cryogenics* - We further examine the cooling of the membrane when it is initially in a cryogenic environment with  $T = 0.1$  K, as shown in Fig. 5. Note that the phonon occupation of the membrane can be of  $10^4$  quanta even at a cryogenic temperature of tens of millikelvin. In contrast to the case of room-temperature environment, here the effect of the back-action force noise  $S_c(\omega)$  can be stronger than that induced by the mechanical thermal noise  $S_Q^{th}(\omega)$ . As a result, the overall noise spectrum is frequency dependent, and the back-action force noise becomes the leading limitation for effective cooling of the membrane, see the inset of the Fig. 5. Again, we find that in the bistable regime  $T_{\text{eff}}$  gradually approaches the local minimum as  $s_1$  or  $s_2$  gets close to the turning points, but the minimal  $T_{\text{eff}}$  in the bistable region can be either at the upper branch or lower branch. This can be understood again in terms of the optomechanical damping rate  $(\gamma_{\text{eff}}(\omega_m) - \gamma_m)$  near the boundary with  $\lambda(\omega_m) = 0$  [as indicated by the dashed-dotted line], but one should note that the effective temperature becomes strongly dependent on the spectra of the input vacuum noise in a cryogenic environment, but not simply relevant to a large  $\gamma_{\text{eff}}(\omega)$  as in the case of the room temperature. Moreover,

we find that, in the monostable regime, the minimum of the effective temperature is given by  $T_{\text{eff}}^{(\text{min})} \approx 20.7 \mu\text{K}$  with  $U/\kappa = 1.78 \times 10^{-12}$  and  $\Delta/\kappa = 0.5$  (i.e.  $\tilde{U}/\kappa = 0.2$ ), which corresponds to the quanta of phonon being less than one, and is about two orders of magnitude less than the case of  $U = 0$ . Despite the parameter condition with respect to  $T_{\text{eff}}^{(\text{min})}$  is located at the monostable region (corresponding to the case of only branch), one can reach ground state cooling under the unresolved sideband regime with  $\kappa = 2\pi \times 1.5 \text{ MHz}$ ,  $\mathcal{P} = 100 \text{ mW}$ , and  $(\omega_m, \gamma_m, g)/\kappa = (0.2, 6.67 \times 10^{-8}, 2.33 \times 10^{-7})$ .

## VI. FURTHER DISCUSSION AND CONCLUSION

In summary, we have studied mechanical cooling at the bistable regime of a dissipative optomechanical cavity with a large linewidth, which is modulated by the mechanical displacement. For appropriate laser driving frequencies, there exists a wide driving-power range on the order of 100 mW for observing optical bistability with  $\kappa/2\pi = 1.5 \text{ MHz}$ . The mechanical membrane can be optimally cooled down to 5 mK from the room temperature in the bistable region at the unresolved sideband regime, and can be cooled down close to the ground state from the cryogenic temperature  $T = 0.1$  K in the monostable region. For further studies, when the cavity linewidth is comparable to the mechanical frequency, one again finds the optimal  $T_{\text{eff}}$  around  $s_{1(2)} \sim 0$  at the bistable regime with  $T = 293$  K. Moreover, increasing the laser driving power enables cooling of the membrane to a lower temperature for a weaker Kerr nonlinearity, however, the laser detuning should be enlarged correspondingly in order to stabilize the system. Since the mechanical cooling strongly depends on the laser detuning and the Kerr nonlinearly modified effective detuning, therefore, the lowest mechanical temperature that can be achieved will be limited by the free spectral range of the cavity. Our result marks a crucial step for understanding the bistable behavior of the dissipative optomechanical systems, and has potential applications in preparation of nonclassical mechanical states and quantum information processing.

## ACKNOWLEDGMENTS

H.W. acknowledges support from the National Natural Science Foundation of China under Grants No. 11774058 and No. 12174058. Y.L. was supported by the Natural Science Foundation of China (Grants No. 12074030 and No. 12274107) and the Research Funds of Hainan University [Grant No. KYQD(ZR)23010].

- 
- [1] M. Aspelmeyer, T. J. Kippenberg, and F. Marquardt, *Rev. Mod. Phys.* **86**, 1391 (2014).
- [2] F. Marquardt, J. G. E. Harris, and S. M. Girvin, *Phys. Rev. Lett.* **96**, 103901 (2006).
- [3] C. Metzger, M. Ludwig, C. Neuenhahn, A. Ortlieb, I. Favero, K. Karrai, and F. Marquardt, *Phys. Rev. Lett.* **101**, 133903 (2008).
- [4] G. Heinrich, M. Ludwig, H. Wu, K. Hammerer, and F. Marquardt, *C. R. Phys.* **12**, 837 (2011).
- [5] H. Wu, G. Heinrich, and F. Marquardt, *New J. Phys.* **15**, 123022 (2013).
- [6] S. Walter, A. Nunnenkamp, and C. Bruder, *Phys. Rev. Lett.* **112**, 094102 (2014).
- [7] L. Mercadé, K. Pelka, R. Burgwal, A. Xuereb, A. Martínez, and E. Verhagen, *Phys. Rev. Lett.* **127**, 073601 (2021).
- [8] M. Ludwig, B. Kubala, and F. Marquardt, *New J. Phys.* **10**, 95013 (2008).
- [9] G. Heinrich, M. Ludwig, J. Qian, B. Kubala, and F. Marquardt, *Phys. Rev. Lett.* **107**, 043603 (2011).
- [10] T. Weiss, A. Kronwald, and F. Marquardt, *New J. Phys.* **18**, 013043 (2016).
- [11] M. Bagheri, M. Poot, L. Fan, F. Marquardt, and H. X. Tang, *Phys. Rev. Lett.* **111**, 213902 (2013).
- [12] T. Carmon, M. C. Cross, and K. J. Vahala, *Phys. Rev. Lett.* **98**, 167203 (2007).
- [13] J. Larson and M. Horsdal, *Phys. Rev. A* **84**, 021804(R) (2011).
- [14] D.-W. Zhang, S.-W. Bin, C. You, and C.-S. Hu, *Opt. Express* **30**, 1314 (2022).
- [15] L. Bakemeier, A. Alvermann, and H. Fehske, *Phys. Rev. Lett.* **114**, 013601 (2015).
- [16] S. Aldana, C. Bruder, and A. Nunnenkamp, *Phys. Rev. A* **88**, 043826 (2013).
- [17] F. Marquardt, J. P. Chen, A. A. Clerk, and S. M. Girvin, *Phys. Rev. Lett.* **99**, 093902 (2007).
- [18] I. Wilson-Rae, N. Nooshi, W. Zwerger, and T. J. Kippenberg, *Phys. Rev. Lett.* **99**, 093901 (2007).
- [19] M. R. Vanner, J. Hofer, G. D. Cole, and M. Aspelmeyer, *Nat. Commun.* **4**, 2295 (2013).
- [20] J. D. Teufel, T. Donner, D. Li, J. W. Harlow, M. S. Allman, K. Cicak, A. J. Sirois, J. D. Whittaker, K. W. Lehnert, and R. W. Simmonds, *Nature (London)* **475**, 359 (2011).
- [21] A. Sawadsky, H. Kaufer, R. M. Nia, S. P. Tarabrin, F. Y. Khalili, K. Hammerer, and R. Schnabel, *Phys. Rev. Lett.* **114**, 043601 (2015).
- [22] J. Chan, T. P. M. Alegre, A. H. Safavi-Naeini, J. T. Hill, A. Krause, S. Gröblacher, M. Aspelmeyer, and O. Painter, *Nature (London)* **478**, 89 (2011).
- [23] A. D. O'Connell, M. Hofheinz, M. Ansmann, R. C. Bialczak, M. Lenander, E. Lucero, M. Neeley, D. Sank, H. Wang, M. Weides, J. Wenner, J. M. Martinis, and A. N. Cleland, *Nature (London)* **464**, 697 (2010).
- [24] J. Qian, A. A. Clerk, K. Hammerer, and F. Marquardt, *Phys. Rev. Lett.* **109**, 253601 (2012).
- [25] M. R. Vanner, M. Aspelmeyer, and M. S. Kim, *Phys. Rev. Lett.* **110**, 010504 (2013).
- [26] J.-Q. Liao and L. Tian, *Phys. Rev. Lett.* **116**, 163602 (2016).
- [27] T. J. Milburn, M. S. Kim, and M. R. Vanner, *Phys. Rev. A* **93**, 053818 (2016).
- [28] J. Li, S. Gröblacher, S.-Y. Zhu, and G. S. Agarwal, *Phys. Rev. A* **98**, 011801(R) (2018).
- [29] I. Shomroni, L. Qiu, and T. J. Kippenberg, *Phys. Rev. A* **101**, 033812 (2020).
- [30] T. A. Palomaki, J. D. Teufel, R. W. Simmonds, and K. W. Lehnert, *Science* **342**, 710 (2013).
- [31] R. Riedinger, A. Wallucks, I. Marinković, C. Löschnauer, M. Aspelmeyer, S. Hong, and S. Gröblacher, *Nature (London)* **556**, 473 (2018).
- [32] I. Marinković, A. Wallucks, R. Riedinger, S. Hong, M. Aspelmeyer, and S. Gröblacher, *Phys. Rev. Lett.* **121**, 220404 (2018).
- [33] N. Fiaschi, B. Hensen, A. Wallucks, R. Benevides, J. Li, T. P. M. Alegre, and S. Gröblacher, *Nat. Photon.* **15**, 817 (2021).
- [34] K. Stannigel, P. Rabl, A. S. Sørensen, P. Zoller, and M. D. Lukin, *Phys. Rev. Lett.* **105**, 220501 (2010).
- [35] D. E. Chang, V. Vuletić, and M. D. Lukin, *Nat. Photon.* **8**, 685 (2014).
- [36] M. A. Nielsen, I. Chuang, and L. K. Grover, *Am. J. Phys.* **70**, 558 (2002).
- [37] K. Stannigel, P. Rabl, A. S. Sørensen, M. D. Lukin, and P. Zoller, *Phys. Rev. A* **84**, 042341 (2011).
- [38] S. Rips and M. J. Hartmann, *Phys. Rev. Lett.* **110**, 120503 (2013).
- [39] A. K. Tagantsev and S. A. Fedorov, *Phys. Rev. Lett.* **123**, 043602 (2019).
- [40] S. M. Meenehan, J. D. Cohen, G. S. MacCabe, F. Marsili, M. D. Shaw, and O. Painter, *Phys. Rev. X* **5**, 041002 (2015).
- [41] C. Fabre, M. Pinar, S. Bourzeix, A. Heidmann, E. Giacobino, and S. Reynaud, *Phys. Rev. A* **49**, 1337 (1994).
- [42] A. Kronwald, F. Marquardt, and A. A. Clerk, *New J. Phys.* **16**, 063058 (2014).
- [43] G. S. Agarwal and S. Huang, *Phys. Rev. A* **93**, 043844 (2016).
- [44] E. E. Wollman, C. U. Lei, A. J. Weinstein, J. Suh, A. Kronwald, F. Marquardt, A. A. Clerk, and K. C. Schwab, *Science* **349**, 952 (2015).
- [45] C.-S. Hu, Z.-B. Yang, H. Wu, Y. Li, and S.-B. Zheng, *Phys. Rev. A* **98**, 023807 (2018).
- [46] N. Aggarwal, T. J. Cullen, J. Cripe, G. D. Cole, R. Lanza, A. Libson, D. Follman, P. Heu, T. Corbitt, and N. Mavalvala, *Nat. Phys.* **16**, 784 (2020).
- [47] K. Kustura, C. Gonzalez-Ballester, A. d. l. R. Sommer, N. Meyer, R. Quidant, and O. Romero-Isart, *Phys. Rev. Lett.* **128**, 143601 (2022).
- [48] R. Ghobadi, A. R. Bahrapour, and C. Simon, *Phys. Rev. A* **84**, 033846 (2011).
- [49] R. Ghobadi, A. R. Bahrapour, and C. Simon, *Phys. Rev. A* **84**, 063827 (2011).
- [50] C.-S. Hu, Z.-Q. Liu, Y. Liu, L.-T. Shen, H. Wu, and S.-B. Zheng, *Phys. Rev. A* **101**, 033810 (2020).
- [51] F. Elste, S. M. Girvin, and A. A. Clerk, *Phys. Rev. Lett.* **102**, 207209 (2009).
- [52] G. S. Agarwal and S. Huang, *Phys. Rev. A* **81**, 041803(R) (2010).

- [53] S. Weis, R. Rivière, S. Deléglise, E. Gavartin, O. Arcizet, A. Schliesser, and T. J. Kippenberg, *Science* **330**, 1520 (2010).
- [54] A. Xuereb, R. Schnabel, and K. Hammerer, *Phys. Rev. Lett.* **107**, 213604 (2011).
- [55] T. Weiss, C. Bruder, and A. Nunnenkamp, *New J. Phys.* **15**, 045017 (2013).
- [56] S. P. Tarabrin, H. Kaufer, F. Y. Khalili, R. Schnabel, and K. Hammerer, *Phys. Rev. A* **88**, 023809 (2013).
- [57] M. Li, W. H. P. Pernice, and H. X. Tang, *Phys. Rev. Lett.* **103**, 223901 (2009).
- [58] M. Wu, A. C. Hryciw, C. Healey, D. P. Lake, H. Jayakumar, M. R. Freeman, J. P. Davis, and P. E. Barclay, *Phys. Rev. X* **4**, 021052 (2014).
- [59] R. M. Cole, G. A. Brawley, V. P. Adiga, R. De Alba, J. M. Parpia, B. Ilic, H. G. Craighead, and W. P. Bowen, *Phys. Rev. Appl.* **3**, 024004 (2015).
- [60] D. Blair, L. Ju, C. Zhao, L. Wen, H. Miao, R. Cai, J. Gao, X. Lin, D. Liu, L.-A. Wu, Z. Zhu, G. Hammond, H. J. Paik, V. Fafone, A. Rocchi, C. Blair, Y. Ma, J. Qin, and M. Page, *Sci. China Phys. Mech. Astron.* **58**, 120405 (2015).
- [61] Y.-X. Zhang, S. Wu, Z.-B. Chen, and Y. Shikano, *Phys. Rev. A* **94**, 023823 (2016).
- [62] X. Y. Zhang, Y. H. Zhou, Y. Q. Guo, and X. X. Yi, *Phys. Rev. A* **100**, 023807 (2019).
- [63] J. D. Teufel, D. Li, M. S. Allman, K. Cicak, A. J. Sirois, J. D. Whittaker, and R. W. Simmonds, *Nature (London)* **471**, 204 (2011).
- [64] W.-J. Gu and G.-X. Li, *Opt. Express* **21**, 20423 (2013).
- [65] Y. Yan, W. Gu, and G. Li, *Sci. China Phys. Mech. Astron.* **58**, 1 (2015).
- [66] K. Qu and G. S. Agarwal, *Phys. Rev. A* **91**, 063815 (2015).
- [67] A. K. Tagantsev, I. V. Sokolov, and E. S. Polzik, *Phys. Rev. A* **97**, 063820 (2018).
- [68] S. Huang and A. Chen, *Phys. Rev. A* **102**, 023503 (2020).
- [69] A. C. Hryciw, M. Wu, B. Khanaliloo, and P. E. Barclay, *Optica* **2**, 491 (2015).
- [70] S. Huang and G. S. Agarwal, *Phys. Rev. A* **95**, 023844 (2017).
- [71] A. Mehmood, S. Qamar, and S. Qamar, *Phys. Rev. A* **98**, 053841 (2018).
- [72] A. Mehmood, S. Qamar, and S. Qamar, *Europhys. Lett.* **131**, 24005 (2020).
- [73] Q. He, F. Badshah, Y. Song, L. Wang, E. Liang, and S.-L. Su, *Phys. Rev. A* **105**, 013503 (2022).
- [74] S. P. Vyatchanin and A. B. Matsko, *Phys. Rev. A* **93**, 063817 (2016).
- [75] M. Ashour, J. N. Caspers, E. M. Weig, and P. Degenfeld-Schonburg, *Phys. Rev. A* **103**, 023513 (2021).
- [76] J. G. Huang, Y. Li, L. K. Chin, H. Cai, Y. D. Gu, M. F. Karim, J. H. Wu, T. N. Chen, Z. C. Yang, Y. L. Hao, C. W. Qiu, and A. Q. Liu, *Appl. Phys. Lett.* **112**, 051104 (2018).
- [77] O. Kyriienko, T. C. H. Liew, and I. A. Shelykh, *Phys. Rev. Lett.* **112**, 076402 (2014).
- [78] K. Pelka, G. Madiot, R. Braive, and A. Xuereb, *Phys. Rev. Lett.* **129**, 123603 (2022).
- [79] C. Genes, D. Vitali, P. Tombesi, S. Gigan, and M. Aspelmeyer, *Phys. Rev. A* **77**, 033804 (2008).
- [80] V. Giovannetti and D. Vitali, *Phys. Rev. A* **63**, 023812 (2001).
- [81] E. X. DeJesus and C. Kaufman, *Phys. Rev. A* **35**, 5288 (1987).